2D ANALYTICAL MODELLING OF DUAL GATE DUAL METAL MoS_2 BASED MOSFET FOR BIOSENSING APPLICATION

RP Murugesh
Department of Electronics and Communication Engineering
Thiagarajar College of Engineering,Madurai,Tamilnadu,India

KG Sanjay Prasanth
Department of Electronics and Communication Engineering
Thiagarajar College of Engineering,Madurai,Tamilnadu,India

M Muthukaruppan
Department of Electronics and Communication Engineering
Thiagarajar College of Engineering,Madurai,Tamilnadu,India

NB Balamurugan
Department of Electronics and Communication Engineering
Thiagarajar College of Engineering,Madurai,Tamilnadu,India

Abstract- In this paper, an analytical model is developed for an MoS2-based double metal double gate (DMDG) MOSFET which is used for the rapid detection of SARs CoV-2 virus biomarker. Using the support of the SILVACO ATLAS TCAD course, parameters such as surface potential, drain current, threshold voltage, and sensitivity are computed and simulated. The virus proteins are speculated to exhibit a dielectric constant of k=4,10,12 and an alteration in DNA charge density of -2x1012 Ccm-2 to 2x1012 Ccm-2. The results obtained show better performance compared to the dual gate single metal Mos2-based MOSFET.

Keywords – MOSFET, covid-19, MOS_2, Biosensors

I. INTRODUCTION

Detecting the novel SARs-CoV-2 (COVID-19) virus as quickly as practical is essential for being able to screen for the highly transmissible respiratory illness that it causes in humans. The fast spread of the COVID-19 epidemic and its wide range of respiratory symptoms, from mild to severe, led the World Health Organization (WHO) to recognize the magnitude of the situation and classify it as a global pandemic. Early discovery and diagnosis are therefore key in the successful management and control of the wide outbreak.

Pursuant to The Centers for Disease Control and Prevention (CDC), USA [1], the envelope (E-Protein) and spike (S-Protein) proteins are attached to the sphere-like form of the SARs-CoV-2 virus, which is characterized by a thin membrane wrapping the virus. The structural depiction of the virus is displayed in Fig. 1(a), particularly emphasizing the RNA genetic material that can be found within the Nucleocapsid proteins (N-Protein). immediate view reverse transcription-polymerase chain reaction (RT-PCR) has recently become the main strategy for finding and managing SARs-CoV-2. To determine the RNA (N-Protein), open frame reading b1 (OFRb1), OFRb2, and E-protein gene, data from nasal swabs must be taken. However, the procedure, that entails the production of viral RNA and takes about three hours, presents obstacles with precise diagnosis [2]. As a result, there is a pressing demand to create one sensitive screening approach capable of rapidly detecting virus antigens in clinical collections without the need for substantial sample preparation, permitting rapid and efficient COVID-19 diagnosis

Field-effect transistor (FET) based biosensors have been shown to be a few of the finest diagnostic techniques accessible with great sensitivity even when quickly measuring a small number of analytes [3, 4]. mainly due to the continued trend of aggressive scaling, Materials which are two-dimensional (2D), such transition metal dichalcogenides (TMDCs), gradually supplanting silicon-based FETs, which are experiencing dipped carrier mobility. These materials have a large bandgap, excellent surface/volume ratio, resilient carrier transportation, thermal stability, and atomistic depth [5,6]. Among TMDC materials, monolayer MoS2 has a smaller indirect band gap of 1.2 eV and an important direct band gap of 1.8 eV, yet bulk MoS2 has an on/off current ratio of around 108.due to its own unique features, namely its elevated mobility of carriers (~100 cm2/Vs) in context.

The present research focuses on a dual gate, dual metal MoS2-based MOSFET for the SARs-CoV-2 virus that has a nanogap included in the gate dielectric. An in-depth examination of the I_{on}/I_{off} ratio, threshold voltage shift, and transfer characteristics has been performed out in a commercial TCAD environment. The S-protein and C-DNA dielectric viral proteins, as well as differed DNA charge densities, have been used to extract threshold voltage sensitivity (Svth). The primary objective of this research is to evaluate the device's sensing ability under various scenarios to demonstrate its applicability for precise quick diagnostic applications.

II. DEVICE DESIGN

As noted in Fig. 2, the DGDM-MoS2-Covid-19 MOSFET is an unusual design for a single nano-gap embedded dual-gate dual-metal MOSFET containing a biosensor based on an ultra-thin Molybdenum Disulfide (MoS2) channel for Covid-19 detection. This design contains an ultra-thin MoS2 channel featuring a 40 nm length and 5 nm thickness. The nano-gap embedded within the gate dielectric is designed to be 30 nm in length and 2 nm in thickness, optimizing the capture and stabilization of bio-elements. The gate dielectric includes a low-k dielectric, SiO2, with a thickness of 1 nm, and a high-k dielectric, HfO2, spanning 3 nm in thickness and 10 nm in length. The highly doped MoS2 channel includes 10^15 cm^-3 N-type impurities, while the significantly N-type doped source and drain regions of the recommended device have impurities of 10^20 cm^-3. Since it is easy to add the SILVACO ATLAS TCAD tool [7,8] into a three-dimensional simulator [9,10], it is the tool of choice for simulating materials with two dimensions. A multiple layers MoS2 channel with an indirect band-gap (Egap) of 1.2 eV, 4.21 eV overall electron affinity (σs) and 8.5 eV overall permittivity is taken into consideration in this simulation. Effective masses for electrons and holes inside the MoS2 channel were 0.52mo and 0.64mo, respectively. In the proposed model, gold is used as metal 1 and silver is used as metal 2.

TABLE 1. DESIGN SPECIFICATION OF DESIGNED DEVICE

Parameter	**Value**
Gate 1 length and Gate 2 length	50nm
Length of the channel(L_{ch})	100nm
Thickness of the channel(t_{si})	10nm
gate oxide length(L_2andL_3)	25nm
Thickness of nanogap(t_{bio})	9nm
Cavity length(L_1 and L_2)	25nm
High-k gate oxide thickness(t_{0x1})	9nm
Gate oxide thickness for low-K(t_{ox2})	1nm
Doping concentration of the channel (N_d)	10^{20} cm^{-3}
Concentration of source and drain(N_{sd})	10^{20} cm^{-3}
Work function of silicon(Φ_{si})	4.3 eV

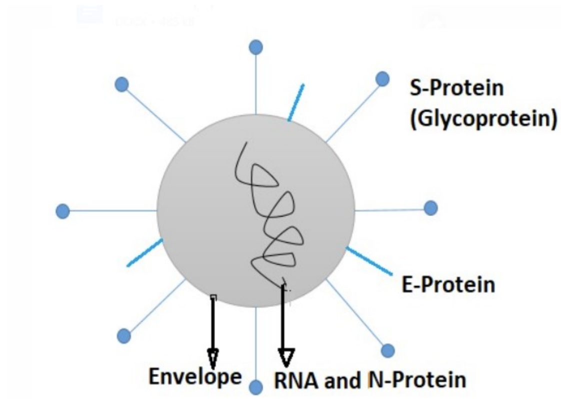

Figure 2 An example of the SARS-CoV-2 virus resulting in Covid-19

Bio-elements with dielectric constants (κ) of 4, 10, and 12 are put inside the put nano-gap to provide the gating effect, replicating the bio sensing mechanism. It is fully explored in Section III. The absence of elements within the nano-gap was demonstrated by κ=1. Across the simulation study, a gate-to-source voltage (VGS) of 1.5V and a drain-to-source voltage (VDS) of 1V is maintained.

Many physical models, which includes Shockley-Read-Hall (SRH) for carrier generation and recombination, Fermi-Dirac, field-dependent mobility (FLDMOB), concentration-dependent mobility (CONMOB), and Band-gap Narrowing (BGN) models for highly doped source and drain regions, have been incorporated to accurately model the device.

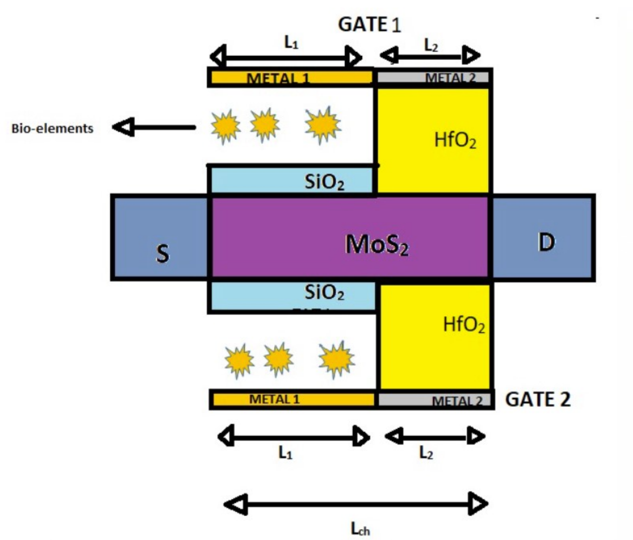

Figure 2 Schematic of dual gate dual metal MoS_2 based MOSFET

III. PARAMETERS MODELING

Each region's potential distribution may seem found by resolving Poisson's equation.

$$\frac{\delta^2 \phi_i(x,y)}{\delta y^2}+\frac{\delta^2 \phi_i(x,y)}{\delta x^2}=\frac{-q\, N_d}{\varepsilon s_i} \qquad (1)$$

With boundary conditions applied in the x and y directions, the Poisson equation is solved independently

i) $0 \le X \le ts_i$, $0 \le y \le Z_1$

ii) $0 \leq X \leq ts_i$, $Z_1 \leq y \leq Z_1+Z_2$
iii) $0 \leq X \leq ts_i$, $Z_1 \leq y \leq Z_1+Z_2+Z_3$
iv) $0 \leq X \leq ts_i$, $Z_1+Z_2+Z_3 \leq y \leq Z_1+Z_2+Z_3+Z_4$

The parabolic approach and the arbitrary constants are utilized to solve for two distinct metals as,

Z_1 and Z_4 represent the length of nano gap cavity
Z_2 and Z_3 represent the length of Gate 1 and Gate 2
Ts_i-> silicon channel

$\phi(x,y)$ is an indication of the 2-D potential of the domains using the parabolic approximation, revealing the potential distribution in each region.

$$\phi(x,y) = a0_i(y)+a1_i(y)+a2_i(Y)x^2 \tag{2}$$

Flat Band Voltage :-

$$Vfb = Vgs-\phi_m-\phi_{si}-\frac{-q\,N_f}{Cb_{io}} \tag{3}$$

$$C_{bio} = \frac{\varepsilon b_{io}}{tb_{io}} \tag{4}$$

We Use:-

$$a_{oi}(y)= \phi_{fsi}(y)$$

$$a_{1i}(y)=\frac{\varepsilon_{bio}/t_{bio}}{\varepsilon_{si}}(\phi_{fsi}(y)- V_{gs}+(V_{gs}-\phi_m-\phi_{si} - \frac{q_{Nf}}{C_{bio}}) \tag{5}$$

$$a_{2i}(y)= \frac{-\varepsilon_{bio}/t_{bio}}{\varepsilon_{si}t_{si}}(\phi fs_i(y)- V_{gs}+(V_{gs}-\phi_m-\phi s_i-\frac{q_{Nf}}{C_{bio}}) \tag{6}$$

$$\phi_i(x,y)= \phi fs_i(y)+ \frac{\varepsilon_{bio}/t_{bio}}{\varepsilon_{si}}(\phi f_{si}(y)- V_{gs} +(V_{gs} -\phi_m-\phi_{si}-\frac{q_{Nf}}{C_{bio}})x-\frac{-\varepsilon_{bio}/t_{bio}}{\varepsilon_{si}t_{si}}(\phi_{fsi}(y)- \quad V_{gs}+(\phi fs_i(y)-$$

$$V_{gs}+(V_{gs}- \phi_m- \phi_{si}-\frac{q_{Nf}}{C_{bio}})x^2 \tag{7}$$

Since punch through current implies ϕc_i (y) to be important, we used x=t_si/2 to determine the relation between ϕc_i (y) & ϕf_si(y). Modify equation 3 using equation 7.

$$\phi fs_i(x,y)=\frac{1}{\frac{1+\frac{\varepsilon_{bio}}{t_{bio}}t_{si}}{4\varepsilon_{si}}}\left\{\phi\,\frac{\varepsilon_{bio}}{t_{bio}}(y)+\frac{\varepsilon_{bio}(t_{si})/t_{bio}}{4\varepsilon_{si}}\left(V_{gs}-V_{gs}-\phi_m-\phi_{si}-\frac{q_{Nf}}{C_{bio}}\right\}\right.$$

$$\frac{\delta^2\phi c_i(y)}{\sqrt{y^2}}-\frac{\phi C_i(y)-V_{gs}+V_{gs}-\phi_m-\phi_{si}-\frac{q_{Nf}}{C_{bio}}}{\eta_i^2}=\frac{-q\,N_d}{\varepsilon s_i} \tag{8}$$

$$[\phi_i(x,y)=\frac{1}{\frac{1+\varepsilon_{bio}}{\frac{t_{bio}}{4\varepsilon_{si}}}t_{si}}\{\phi\,c_i\,(y)+\frac{\frac{\varepsilon_{bio}}{t_{bio}}t_{si}}{4\varepsilon_{si}}(V_{gs}-V_{gs}-\phi_m-\phi_{si}-\frac{q_{Nf}}{C_{bio}})\}(1+\frac{\frac{\varepsilon_{bio}}{t_{bio}}}{\varepsilon_{si}}+\frac{\frac{\varepsilon_{bio}}{t_{bio}}}{\varepsilon_{si}\,t_{si}}x^2)-$$

$$\frac{\frac{\varepsilon_{bio}}{t_{bio}}}{\varepsilon_{si}}(V_{gs}-V_{gs}-\phi_m-\phi_{si}-\frac{q_{Nf}}{C_{bio}})x+\frac{\frac{\varepsilon_{bio}}{t_{bio}}}{c_{si}\,t_{si}}(V_{gs}-V_{gs}-\phi_m-\phi_{si}-\frac{q_{Nf}}{C_{bio}})x^2\,] \tag{9}$$

Where,

$$\eta_i=\sqrt{\frac{4\,\varepsilon_{si}\,t_{si}+\frac{\varepsilon_{bio}}{t_{bio}}t^2{}_{si}}{8\,\frac{\varepsilon_{bio}}{t_{bio}}}} \tag{10}$$

The general solution of eqn (8) is written as

$$\phi ci\,(y)=A_{ie}\,\frac{y}{\eta_i}+B_{ie}\,\frac{-y}{\eta_i}+\sigma_j \tag{11}$$

$$\sigma_I=\eta^2{}_i\,\frac{q\,N_d}{\varepsilon s_i}-(V_{gs}-V_{gs}-\phi_m-\phi_{si}-\frac{q_{Nf}}{C_{bio}}) \tag{12}$$

A_i & B_i are coefficients obtained by using the boundary condition

$$\phi\,c_i\,(o)=V_{bi}$$

$$\phi\,c_i\,(Z_1+Z_2+Z_3+Z_4)=V_{bi}+V_{ds} \tag{13}$$

$$V_{bi}=V_t\,\mathrm{In}\,\frac{N_d}{\eta_i}$$

$$S_1=\frac{(V_{bi-\sigma_1})\,e^{\frac{z1}{\eta_1}}-(\psi_{1-\sigma1})}{2\sinh\frac{z_1}{\sigma I}} \tag{14}$$

$$C_1=(V_{bi}\text{-}\sigma_1\text{–}B_1)$$

$$S_2=\frac{(\psi-\sigma2)e^{\frac{z1}{\eta_2}}-(\psi_{1-\sigma2})}{2\sinh(\frac{z_2}{\eta_2})\,e^{\frac{-z1}{\eta_2}}} \tag{15}$$

$$C_2=\frac{(\psi-\sigma2)-B_2\,e^{\frac{-z1}{\eta_2}}}{e^{\frac{-z1}{\eta_2}}} \tag{16}$$

$$S_3=\frac{(\psi_2-\sigma3)e^{\frac{z3}{\eta_3}}-(\psi_{3-\sigma3})}{2\sinh(\frac{z_3}{\eta_3})\,e^{\frac{-z1-z2}{3}}} \tag{17}$$

$$C_3=\frac{(\psi_2-\sigma3)-B_3\,e^{\frac{-z1-z2}{\eta_3}}}{e^{\frac{z1+z2}{\eta_2}}} \tag{18}$$

$$S_4=\frac{(\psi_3-\sigma4)e^{\frac{z4}{\eta_4}}\;-(V_{bi-V_{ds}-\sigma4})}{2\sinh(\frac{z_3}{\eta_3})\,e^{\frac{-z1-z2-z3}{\eta_3}}} \tag{19}$$

$$C_4=\frac{(\psi_3-\sigma4)-B_4\,e^{\frac{-z1-z2-z3}{\eta_3}}}{e^{\frac{z1+z2+z3}{\eta_4}}} \tag{20}$$

here V_{bi} is $\psi_1,\psi_2,\psi_3,$ are the intermediate potentials

$$\phi_1 \quad (u, v) = c_{01}(v) + c_{11}(v)(u) + c_{21}(v)u^2 \tag{21}$$
$$\phi_2 \quad (u, v) = c_{02}(v) + c_{12}(v)(u) + c_{22}(v)u^2 \tag{22}$$
$$\phi_3 \quad (u, v) = c_{03}(v) + c_{13}(v)(u) + c_{23}(v)u^2 \tag{23}$$
$$\phi_4 \quad (u, v) = c_{04}(v) + c_{14}(v)(u) + c_{24}(v)u^2 \tag{24}$$

where $\phi(u, v) = \phi(u, v)$ for $0 \le v \le L1$ (25)

$\phi(u,v) = \phi_{2(u,v)}$ for $z1 \le y \le z1+z2$

$\phi(u,v) = \phi_{3(u,v)}$ for $z1+z2 \le y \le z1+z2+z3$ (26)

$\phi(u,v) = \phi_{4(u,v)}$ for $z1+z2+z3 \le y \le z1+z2+z3+z4$ (27)

drain current in subthreshold region can be written as

$$I_{d\ sub} = \frac{\mu_{WKT\left(1-e^{\frac{-qV_{ds}}{kT}}\right)}}{\sum_{i=1}^{4}\int_0^{L_i}\frac{1}{\int_0^{t_{si}} n_{ie^{\frac{q\phi_{i(x,y)}}{KT}}}dx}dy} \tag{28}$$

drain current in region 1 is,

$$I_{d\ linear\ 1} = \frac{\mu\ WC_1}{L_1}\left(\left(V_{gs-V_{th}}\right)V_{P1-\frac{V^2P_1}{2}}\right. \tag{29}$$

The drain current in region 2 is,

$$I_{d\ linear\ 2} = \frac{\mu\ WC_1}{L_1}\left(\left(V_{gs-V_{th}}\right)\left(V_{p2} - V_{p1}\right) - \left(\frac{V^2p_{2-V^2{}_{P1}}}{2}\right)\right. \tag{30}$$

Region 3 holds the drain current of the DMDG-JL-MOSFET, resulting in a channel length of L3, the drain-tosource voltage is

$$I_{d\ linear\ 3} = \frac{\mu\ WC_3}{L_3}\left(\left(V_{gs-V_{th}}\right)\left(V_{p3} - V_{p2}\right) - \left(\frac{V^2p_{3-V^2{}_{P2}}}{2}\right)\right. \tag{31}$$

Drain and in region 4,

$$I_{d\ linear\ 4} = \frac{\mu\ WC_4}{L_4}\left(\left(V_{gs-V_{th}}\right)\left(V_{ds} - V_{p3}\right) - \left(\frac{V^2d_{3-V^2{}_{P3}}}{2}\right)\right. \tag{32}$$

For each of the four current equations in the quadratic equation, receive the values of VP1–VP2 and VP3.

$$V_{p1}^2R_1 + V_{p1}\ R_2 + R_3 = 0 \tag{33}$$

$$V_{p2}^2A_1 + V_{p2}\ A_2 + A_3 = 0 \tag{34}$$

$$V_{p3}^2Q_1 + V_{p3}\ Q_2 + Q_3 = 0 \tag{35}$$

Where,

$$M_1 = \frac{-1}{2}\left(\frac{g_1}{z_1} + \frac{g_2}{z_2}\right) \tag{36}$$

$$M_2 = \frac{g_1}{z_1}(V_{gs}-V_{th}) + \frac{g_2}{z_2}(V_{gs}-V_{p1}) \tag{37}$$

$$M_3 = \frac{g_2}{z_2}\frac{V^2{}_{p2}}{2} - \frac{g_2}{z_2}(V_{gs}-V_{th})V_{p2} \tag{38}$$

$$N_1 = \frac{-1}{2}\left(\frac{g_2}{z_2} + \frac{g_3}{z_3}\right) \quad (39)$$

$$N_2 = \frac{g_2}{z_2}(V_{gs} - V_{th}) + \frac{g_3}{z_3}(V_{gs} - V_{th}) \quad (40)$$

$$N_3 = \frac{g_2}{z_2}\frac{V^2{}_{p2}}{2} - \frac{g_2}{z_2}(V_{gs} - V_{th}) V_{p1} + \frac{g_3}{z_3}\frac{V^2{}_{p3}}{2} - \frac{g_3}{z_3}(V_{gs} - V_{th}) V_{p3} \quad (41)$$

$$Q_1 = \frac{-1}{2}\left(\frac{g_3}{z_3} + \frac{g_4}{z_4}\right) \quad (42)$$

$$Q_2 = \frac{g_3}{z_3}(V_{gs} - V_{th}) + \frac{g_4}{z_4}(V_{gs} - V_{th}) \quad (43)$$

$$Q_3 = \frac{g_3}{z_3}\frac{V^2{}_{p2}}{2} - \frac{g_3}{z_3}(V_{gs} - V_{th}) V_{p2} + \frac{g_4}{z_4}\frac{V^2{}_{ds}}{2} - \frac{g_4}{z_4}(V_{gs} - V_{th}) V_{ds} \quad (44)$$

IV. Results and Discussion

The simulation results between double metal double gate (DMDG) and single metal dual gate (SMDG) MOSFET is compared. In comparing the DMDG MOSFET with the SMDG MOSFET, Fig. 3 displays the drain current compared to the gate voltage plot. Comparing to the SMDG MOSFET, the DMDG MOSFET has better drain current characteristics [11]. This is so that the gate voltages applied to each gate may be independently regulated when there are two distinct metallic gates. Better gate control might result from this, decreasing the likelihood of gate leakage and raising the transistor's overall efficiency.

Figure 4 displays the ION/IOFF ratio for the neutral bio-elements. As the dielectric constant values rise,[12] the ratio likewise rises. The device designed by the user has a higher ratio than the SMDG MOSFET. Fig. 5 displays the ION/IOFF ratio for the charged bio-elements. As one reaches Nc=2x1012 Ccm-2, Since there is an uptick in IOFF, the ratio drops for the charged bio-elements. However, the degradation is lesser for DMDG MOSFET [13] compared to SMDG MOSFET.

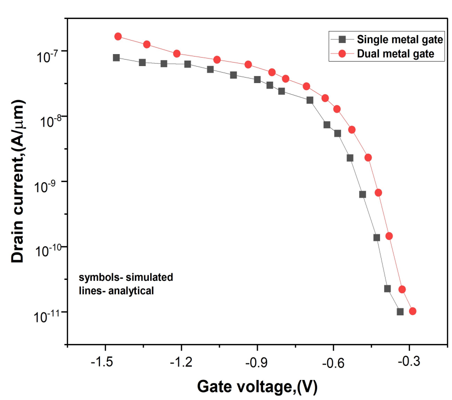

Figure 3 DMDG and SMDG MOSFET drain current profile

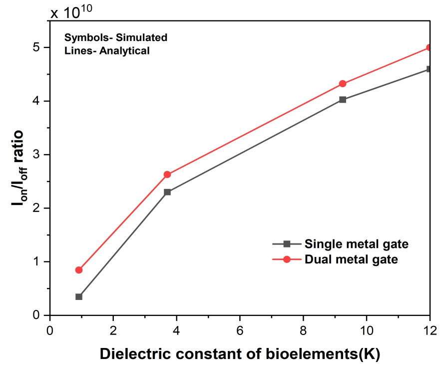

Figure 4 I_{ON}/I_{OFF} ratio profile for the neutral bio-elements

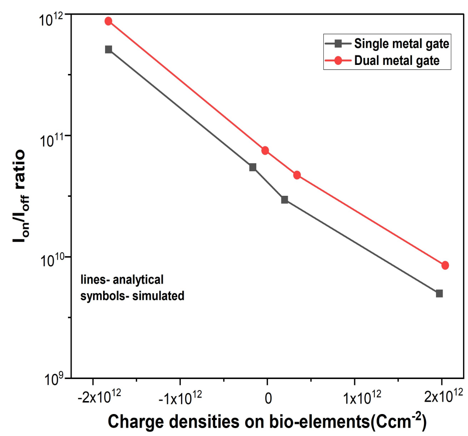

Figure 5 I_{ON}/I_{OFF} ratio profile for the charged bio-elements

Figure 6 and 7 displays the threshold voltage profile of the SMDG and DMDG MOSFET for neutral and charged bio-elements respectively. For the neutral bio-elements the V_{th} increases with an increase in the dielectric constant values threshold voltage of the proposed device is better than the SMDG MOSFET because of suppressed I_{OFF} at k=10,12 values. For the charged bio-elements the threshold voltage degrades for the charged Bio- elements due to an increase in I_{OFF} towards Nc=2x10^{12} Ccm^{-2}. However the degradation is lesser for DMDG MOSFET compared to SMDG MOSFET

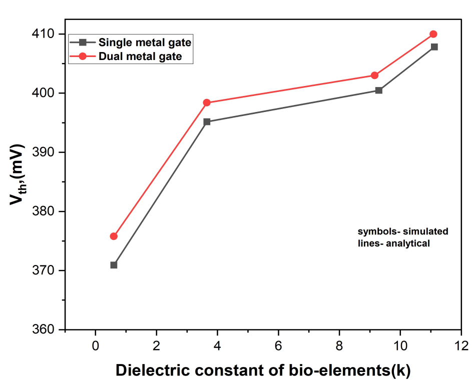

Figure 6 Threshold voltage profile for SMDG and DMDG MOSFET for neutral bio-elements

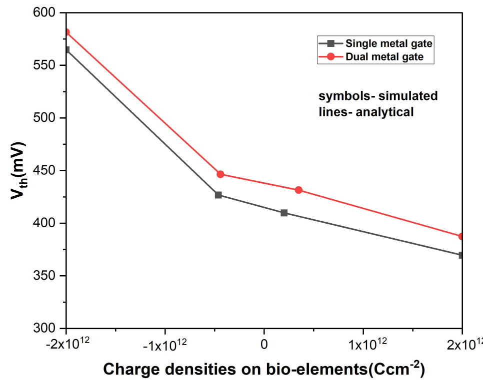

Figure 7 Threshold voltage profile for SMDG and DMDG MOSFET for charged bio-elements

Fig 8. displays the difference between the recommended MoS2-based DMDG MOSFET and the MoS2-based SMDG MOSFET in terms of threshold voltage sensitivity. The dual metal, dual gate MoS2 MOSFET is preferable to the single metal, dual gate MoS2 MOSFET in terms of COVID-19 illness detection due to its unique features. The suggested device obtained a maximum sensitivity of 105 mV, which is better than that of a single metal, dual-gate MOSFET.

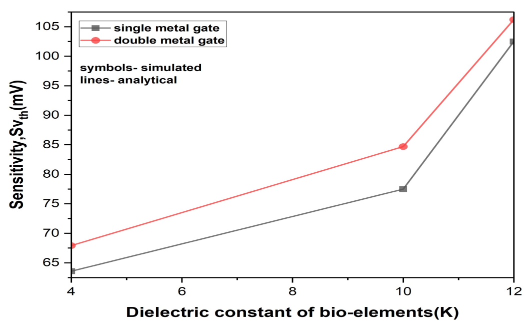

Figure 8 Comparison of threshold voltage sensitivity of proposed DMDG MoS_2 based MOSFET and SMDG MoS_2 based MOSFET

V.CONCLUSION

This work builds a MoS2-based dual metal dual gate MOSFET to detect the Covid-19 virus that causes SARs-CoV-2 in clinical samples. To assess the way the suggested device performs, simulation work and an analytical model are used. In order to validate the effectiveness of identifying the COVID-19 virus, a thorough evaluation of Using a range of DNA charge densities and dielectric viral proteins (such as S-protein and DNA) [14], the effectiveness of the device was assessed. This examination took place using the SILVACO TCAD tool. When it pertains to COVID-19 viral detection and sensitivity, the recommended DMDG MoS2-based MOSFET surpasses the SMDG MoS2-based MOSFET.

REFERENCES

[1] https://emergency.cdc.gov/recentincidents/

[2] SARS-CoV-2 RNA, Qualitative Real-Time RT-PCR (Test Code 39433) Package Insert For Emergency Use, pp. 1–18, [https://www.fda.gov/media/136231/download]

[3] Janissen, R.; Sahoo, P. K.; Santos, C. A.; da Silva, A. M.; von Zuben, A. A. G.; Souto, D. E. P.; Costa, A. D. T.; Celedon, P.;Zanchin, N. I.T.; Almeida, D. B.; Oliveira, D. S.; Kubota, L. T.; Cesar, C. L.; Souza,A. P.; Cotta, M. A. InP Nanowire Biosensor with TailoredBiofunctionalization: Ultrasensitive and Highly Selective DiseaseBiomarker Detection. Nano Lett. 2017, 17, 5938−5949.

[4] Liu, J.; Chen, X.; Wang, Q.; Xiao, M.; Zhong, D.; Sun, W.;Zhang, G.; Zhang, Z. Ultrasensitive Monolayer MoS2 Field-Effect Transistor Based DNA Sensors for Screening of Down Syndrome. Nano Lett.2019, 19, 1437−1444.

[5] F. Schwierz, J. Pezoldt, and R. Granzner, “Two-dimensional materials and their prospects in transistor electronics,” Nanoscale, vol. 7, no. 18,pp. 8261–8283, Apr. 2015.

[6] Kim, J. H., Kim, T. H., Lee, H., Park, Y. R., Choi, W., & Lee, C. J.(2016). Thickness-dependent electron mobility of single and few-layerMoS2 thin-film transistors. Aip Advances, 6(6), 065106.

[7] Manual, A. U. (2000). Silvaco International. Santa Clara, CA, 95054, 23.

[8] Kumari, M., Singh, N. K., & Sahoo, M. (2022). A detailed investigation of dielectric-modulated dual-gate TMD FET based label free biosensor via analytical modelling. Scientific Reports, 12(1), 21115.

[9] Nam, H., Oh, B. R., Chen, P., Yoon, J. S., Wi, S., Chen, M., ... & Liang, X. (2015). Two different device physics principles for operating MoS2 transistor biosensors with femtomolar-level detection limits. Applied Physics Letters, 107(1), 012105.

[10] Wangkheirakpam, V. D., Bhowmick, B., & Pukhrambam, P. D. (2022). Detection of SARS-CoV-2 using dielectric modulated TFET-based biosensor. Journal of Materials Science: Materials in Electronics, 33(13), 10323-10334.

[11] R. Ghosh, S. Sarkhel and P. Saha.(2023).MoS2-Based Dual-Gate mosfet as Ultrasensitive SARs-CoV-2 Biosensor for Rapid Screening of Respiratory Syndrome. IEEE Sensors Letters, vol. 7, no. 11, pp. 1-4.

[12] Yadav, S., Gedam, A., & Tirkey, S. (2020). A dielectric modulated biosensor for SARS-CoV-2. IEEE Sensors Journal, 21(13), 14483-14490.

[13] Kumari, M., Singh, N. K., Sahoo, M., & Rahaman, H. (2021). Work function optimization for enhancement of sensitivity of dual-material (DM), double-gate (DG), junctionless MOSFET-based biosensor. Applied Physics A, 127, 1-8.

[14] Kumar, S., Chauhan, R. K., & Kumar, M. (2022). Sensitivity enhancement of dual gate FET based biosensor using modulated dielectric for Covid detection. Silicon, 1-10.